SPANWISE WALL OSCILLATIONS FOR DRAG REDUCTION, WITHOUT WALLS

K. Vieths
Institute of Fluid Mechanics
Karlsruhe Institute of Technology
76131 Karlsruhe
karl.vieths@kit.edu

D. Gatti
Institute of Fluid Mechanics
Karlsruhe Institute of Technology
76131 Karlsruhe
davide.gatti@kit.edu

M. Quadrio
Department of Aerospace Science and Technology
Politecnico di Milano
20156 Milano
maurizio.quadrio@polimi.it

ABSTRACT

The reduction of skin friction drag in turbulent flows has constituted a significant field of research over the past few decades. Spanwise forcing represents one of the most extensively studied techniques for the reduction of turbulent drag. Even though the performance of such technique has been widely studied and verified (Quadrio & Ricco (2004)), the underlying working principle remains unclear. The prevailing hypothesis is that the reduction in skin friction is a consequence of the interaction between the Stokes layer, i.e. the unsteady spanwise velocity profile created by wall oscillations, and the turbulent motions in the vicinity of the wall. The issue, however, is that in the near wall regions, turbulence is significantly influenced by the presence of the wall itself, which makes it challenging to isolate the impact of wall oscillations on the turbulent structures. The present work proposes that this obstacle may be overcome by removing the wall effect entirely. To achieve this, spanwise forcing is not applied in a canonical wall bounded flow, but in homogeneous shear turbulence instead. Results show similarities with the conventional wall bounded flow performance of spanwise forcing. In particular, an optimum forcing period may be found, corresponding to specific turbulent time scales, i.e. the eddy turnover time. The influence on several statistical quantities, commonly used to describe the behavior of turbulent flows is studied.

INTRODUCTION

The simplest form of spanwise forcing is represented by the so-called spanwise wall oscillations, i.e. the harmonic spanwise movement of a uniform surface, first introduced by Jung *et al.* (1992). The spanwise velocity of the wall is prescribed as:

$$V_{wall} = A\cos(\omega t) \tag{1}$$

where A is the maximum wall velocity, $\omega = 2\pi/T$ and T is the forcing period.

Different studies (e.g., Quadrio & Ricco (2004)) have demonstrated that, if the forcing parameters (i.e., amplitude and period of oscillation) are chosen properly, a reduction of up to 45% in skin friction may be achieved. In particular, the optimal forcing period is $T^+ \approx 100$, where $^+$ denotes viscous wall units computed using the reference skin friction velocity, u_τ. However, the underlying working principle of spanwise forcing remains unclear. It has been proposed that drag reduction is a consequence of a decrease in production of turbulent kinetic energy (e.g, Agostini *et al.* (2014)) or of an increase in dissipation (e.g., Ricco *et al.* (2012)). Different researchers rather concentrated on the role of pressure-strain interactions (e.g., Xu & Huang (2004)). These effects were also related to modifications to the turbulent structures close to the wall caused by the Stokes layer (e.g., Touber & Leschziner (2012), Yakeno *et al.* (2014) or Agostini *et al.* (2015)).

The prevailing hypothesis is that the reduction in skin friction is a consequence of the interaction between the Stokes layer, i.e. the unsteady spanwise velocity profile created by wall oscillations (Quadrio & Sibilla (2000)), and the turbulent motions in the vicinity of the wall. The Stokes layer is given by

$$V_{SL}(z,t) = A\exp(-z/\delta_{SL})\cos(\omega t - z/\delta_{SL}) \tag{2}$$

where z denotes the wall-normal coordinate, $\delta_{SL} = \sqrt{2\nu/\omega}$ is a measure of the Stokes layer thickness and ν is the kinematic viscosity.

In the near wall regions turbulence is significantly influenced by the presence of the wall itself, thus complicating the identification of the wall oscillations' impact. This prompted the idea of removing the wall entirely, by introducing spanwise forcing not in a canonical wall-bounded flow, but in homogeneous shear turbulence (HST) instead. HST is an idealized turbulent flow, characterized by a uniform mean velocity gradient S. It has been shown (e.g. Lee *et al.* (1990), Pumir (1996), Sekimoto *et al.* (2016) or Dong *et al.* (2017)) that HST shares many of the physical aspects of conventional wall-bounded flows, including those interactions responsible for turbulent

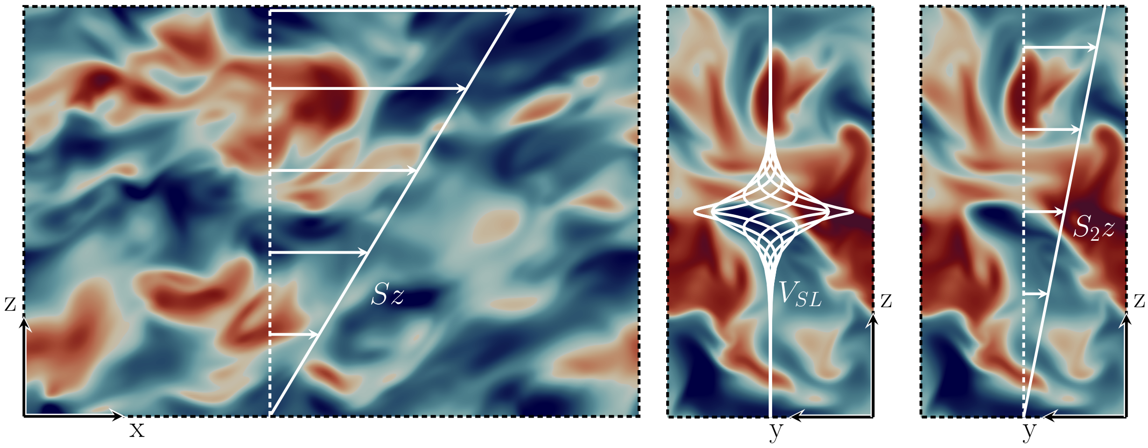

Figure 1: Left to right: mean shear S in (x,z) plane; spanwise forcing in HST-SL cases; spanwise forcing in HST-S2 cases.

kinetic energy production and, ultimately, skin friction drag (Fukagata *et al.* (2002)). However, since the mean velocity gradient is uniform, the flow is statistically homogeneous in all directions (Rogallo, 1981), as the name suggests.

METHOD

Spanwise forcing without walls is investigated through direct numerical simulations (DNS), performed using a purposely developed code, based on the turbulent channel flow code by Luchini & Quadrio (2006) and written in CPL programming language (Luchini (2021)).

As reported by Rogallo (1981), HST is homogeneous in the shearing coordinate system, i.e. $\xi = x - Szt$, $\eta = y$ and $\zeta = z$, where x, y and z are the streamwise, spanwise and vertical coordinates, depicted in Fig. 1. Hence, in the (ξ,η,ζ) coordinate system would be possible to use Fourier expansions along all three directions (e.g. Rogallo (1981)). Instead, if the non-shearing (x,y,z) coordinate system is used, a different approach is needed, e.g. the one proposed by Sekimoto *et al.* (2016). Since x and y are homogeneous also in the non-shearing reference system, Fourier expansions can be used. Along z, fourth-order compact finite differences are employed, in combination with a “shear-periodic” boundary condition. The idea of shear-periodicity is that flow properties are periodic between pairs of points, on the lower and upper boundaries, that are shifted in time by the mean shear. In the present work, the governing equations are discretized in space using the latter.

Time integration is performed through a partially implicit method: linear terms are integrated using a second-order Crank-Nicholson scheme, while a third-order Runge-Kutta scheme is used for the nonlinear ones. Finally, since in HST the mean velocity field is simply given by $(U,V,W) = (Sz,0,0)$, the mean convection terms can be analytically integrated, thus decoupling the CFL condition from the mean flow and increasing the maximum allowable Courant number (Sekimoto *et al.* (2016)).

Numerical simulations of HST are performed by setting the two aspect ratios of the computational box, i.e. $A_{xy} = L_x/L_y$ and $A_{zy} = L_z/L_y$, and the Reynolds number $Re_y = SL_y^2/\nu$. The two aspect ratios must be chosen carefully. Ideal HST, that would require an unbounded domain, grows indefinitely both in intensity and length scale. In numerical simulation the domain is clearly finite, thus constraining the length scale of turbulence. This is what allows HST to reach a steady state (Pumir (1996)), but clearly poses the question on how the domain geometry influences turbulence. It was demonstrated that the relevant domain size is the spanwise one, i.e. L_y, and that by selecting $A_{xy} > 2$ and $A_{zy} > 1$ turbulence becomes independent of the domain's geometry (Sekimoto *et al.* (2016)). This allows comparisons between such flow and realistic wall-bounded flows.

Table 1: Comparison between new and published (Sekimoto *et al.* (2016)) results for HST.

Variable	Current	Sekimoto *et al.* (2016)
Re_λ	47.1	47
S^*	6.785	6.82
I_1	0.0915	0.092
I_2	0.1034	0.104

The DNS code was validated by replicating the case denoted as L32 in Sekimoto *et al.* (2016), with the following parameters: $A_{xy} = 3$, $A_{zy} = 2$ and $Re_y = 2000$. $N_x = 190$ and $N_y = 94$ modes along the homogeneous directions and $N_z = 192$ uniformly spaced points along the vertical one are used for the spatial discretization. Results are reported in Tab. 1. $Re_\lambda = 2k\sqrt{5/(3\nu\varepsilon)}$ is the Taylor-microscale Reynolds number, $S^* = 2Sk/\varepsilon$ is the Corrsin parameter, while I_1 and I_2 are the two Lumley invariants. In the previous formulas, k and ε are the turbulent kinetic energy and the dissipation rate of turbulent kinetic energy, respectively.

The investigation of spanwise forcing in HST is performed following two different strategies. In the first approach, denoted as HST-SL, the Stokes layer's velocity profile (Eq. 2), is enforced directly in the HST flow. The second strategy, instead, involves imposing a uniform spanwise shear to reproduce the effects of spanwise forcing, and will be referred to as HST-S2.

HST-SL cases

In the HST-SL cases, it was chosen to set the Stokes layer at half of the box height, i.e. at $z = \delta = L_z/2$ (Fig. 1). Starting from Eq. 2, the enforced spanwise profile is:

$$V_{SL} = A \exp[-g(z-\delta)/\delta_{SL}] \cos[\omega t - g(z-\delta)/\delta_{SL}] \quad (3)$$

where $g(z-\delta) = |z-\delta|$ represents the absolute value function. From Eq. 3 it is clear that, in general, the actuation parameters would be two in this case, i.e. A and T, since $\delta_{SL} = \sqrt{2\nu/\omega}$. However, in the present work, it was decided to treat δ_{SL} as an independent parameter. From an implementation point of view, the Stokes layer is introduced by imposing that the $(k_x, k_y) = (0,0)$ mode of the spanwise velocity is equal to Eq. 3.

With this approach, the spanwise velocity profile enforced in the HST flow is inhomogeneous in the vertical direction. Indeed, some authors proposed that the second derivative in z of the spanwise velocity profile played a relevant role in the drag reduction mechanism (e.g., Duque-Daza *et al.* (2012)). However, imposing the Stokes layer in HST with this approach has some limitations. First, since the flow becomes inhomogeneous in the z direction, the comparison between the controlled and uncontrolled cases and, ultimately, the identification of the forcing's effect become more difficult. Second, the Stokes layer introduces a vertical length scale, denoted in Eq. 2 as δ_{SL}, which is related to its thickness. However, since the uncontrolled flow is statistically homogeneous in z, there is no natural length scale for δ_{SL} to be compared to. Hence, it is unclear which values of δ_{SL} may be physically relevant.

A total of six simulations are performed with this approach. The Stokes layer's amplitude and thickness are fixed, i.e. $A^+ = 12$ and $\delta_{SL}^+ = 5.64$ (value computed using the classical $\delta_{SL} = \sqrt{2\nu/\omega}$, with $T^+ = 100$), while the period is varied, i.e. $T^+ = 50$, 100, 200, 300, 400, 800. With $()^+$ viscous units, computed using the uncontrolled value of u_τ, are denoted. These cases will be denoted as HST-SL. All HST-SL cases are run with the same numerical parameters as the validation run. Once the initial transient was discarded, statistics were sampled over a duration of $ST_{stat} \approx 1400$.

HST-S2 cases

Given the limitations of the first approach, the HST-S2 strategy is tested. In general, the only requirement for homogeneous shear turbulence is for the mean shear tensor, $S_{ij} = \partial U_i/\partial x_j$, to be spatially uniform and compatible with continuity, i.e. $S_{ii} = 0$, (Rogallo (1981)). Besides that, as reported by Rogallo (1981), S_{ij} could be any function of time. Starting from this observation, the idea behind this second approach is to represent the effect of spanwise forcing through a time-dependent (but spatially uniform) spanwise shear, i.e. $S_{23} = \partial V/\partial z = S_2(t)$ (Fig. 1). In analogy with Eq. 2 and 3, a harmonic spanwise shear is considered, i.e.:

$$S_2(t) = A_{S_2} \sin(\omega_{S_2}\, t) \quad (4)$$

Hence, in this case there are only two actuation parameters, i.e. A_{S_2} and T. In the following, the nondimensional forms, i.e. T^+ and $S_r = A_{S_2}/S$, will be used. Since the spanwise shear prescribed by Eq. 4 is uniform, the flow will be statistically homogeneous in all directions also in the controlled case. This significantly reduces the complexity of the flow's statistics and avoids the ambiguity related to δ_{SL}. These cases will be denoted as HST-S2.

A total of 15 simulations (including an uncontrolled case, to be used as reference) with the HST-S2 approach were run. The actuation parameters were: $T^+ \approx 32, 64, 128, 192, 256$ for $S_r = 0.5, 1.0$ and $T^+ \approx 32, 128, 192, 256$ for $S_r = 2.0$. All HST-S2 cases are run with $Re_y = 1000$, $A_{xy} = 3$ and $A_{zy} = 2$. The spatial discretization uses $N_x = 96$ and $N_y = 32$ modes along the homogeneous directions and $N_z = 64$ uniformly spaced points along the vertical one. Only the case with $S_r = 2$ and $T^+ \approx 256$ required a higher resolution, with $N_x = 120$, $N_y = 40$ and $N_z = 80$. Once the initial transient was discarded, statistics were sampled over a duration of $ST_{stat} \approx 2000$.

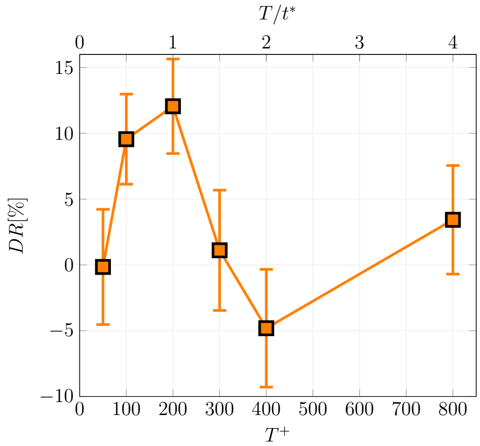

Figure 2: DR in HST-SL as a function of T^+. Vertical bars: the extended uncertainty with 95% confidence level.

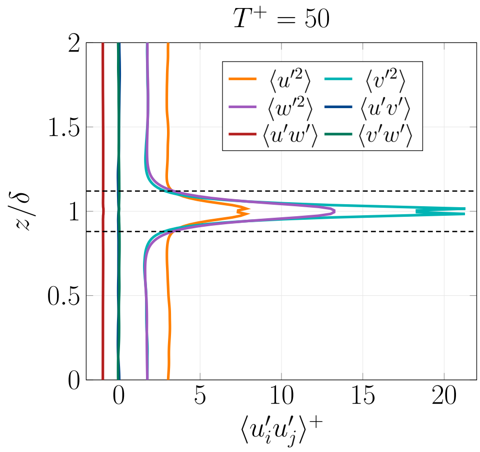

Figure 3: Reynolds stresses' profiles for the $T^+ = 50$ HST-SL case. Dashed lines at $z = \delta \pm \delta_{99} \approx \delta \pm 4.6\delta_{SL}$.

RESULTS

Drag reduction in HST

The performance of a turbulent flow control technique is usually measured in terms of drag reduction, which requires the definition of a friction coefficient. While in wall-bounded flows skin-friction drag can be easily defined, in HST, because of the absence of the walls, it is not straightforward. Sekimoto *et al.* (2016) suggest that the friction velocity u_τ may be defined in HST using the total shear stress, i.e. $u_\tau^2 = \nu S - \overline{uw}$. Here, the lower-case letters u and w denote fluctuations in velocity in the stream and vertical direction, while the operator $\overline{()}$ designates an averaging, in all spatial directions and in time. Indeed, Sekimoto *et al.* (2016) showed that velocity fluctuations in HST scale well with u_τ.

Since it involves averaging in all spatial directions, the definition of u_τ by Sekimoto *et al.* (2016) applies naturally to the cases HST and HST-S2 (due to homogeneity). Regarding the HST-SL cases, the mean streamwise momentum equation may be exploited to demonstrate that the total shear stress must remain uniform over the whole domain's height, even after the introduction of a Stokes layer. Hence, the definition of u_τ by Sekimoto *et al.* (2016) remains valid also in HST-SL cases and a friction coefficient may be defined as:

$$c_f = 2\left(\frac{u_\tau}{U_{ref}}\right)^2 = \frac{8}{A_{zy}^2 Re_y} - \frac{8}{A_{zy}^2}\frac{\overline{uw}}{S^2 L_y^2} \qquad (5)$$

with $U_{ref} = SL_z/2$ and $\overline{uw}$ is the Reynolds shear stress. In the following $c_{f,0}$ represents the c_f in the reference uncontrolled case.

HST-SL cases

Fig. 2 shows that drag reduction, $DR = 1 - c_f/c_{f,0}$, varies non-monotonically with T and an optimum forcing period may be found, as in a conventional wall-bounded setup. An interesting result is that this optimum T corresponds to a specific time scale, i.e. the eddy turnover time $t^* = 2k/\varepsilon$, measured in the uncontrolled case. This is the time scale of larger turbulent structures present in the flow (Lee *et al.* (1990)). This result is consistent with the fact that, in a turbulent shear flow, only "larger" structures (more specifically, with length scales $l > L_c$, with $L_c = \sqrt{\varepsilon/S^3}$) can couple with the mean shear, thus contributing to the production of turbulent kinetic energy (Corrsin (1958), Gualtieri *et al.* (2002)). Hence, it is reasonable to expect that the suppression of $\overline{uw}$, itself related to the production of turbulent kinetic energy, may be related to the interaction between spanwise shear and larger structures.

Fig. 3 reports the Reynolds stresses profiles for the $T^+ = 50$ HST-SL case. The introduction of the Stokes layer defines two regions in the flow: inside the Stokes layer, the normal stresses show large peaks; outside, they remain uniform as in the unforced case. Instead, the shear stress $\langle u'w' \rangle$ remains uniform over the whole domain. The $\langle\rangle$ operator denotes averaging in x, y and time, while $()'$ designates a stochastic fluctuation. This is a relevant distinction for the HST-SL cases, in which temporal fluctuations include not only the stochastic components, but also the deterministic contribution due to the Stokes Layer (Eq. 3).

In steady-state HST, the Reynolds stresses' budgets (Mansour *et al.* (1988)) involve three processes: production P_{ij}, dissipation ε_{ij} and pressure-strain Π_{ij}. In general, when an active control strategy is used, terms related to the power introduced in the flow by the forcing will appear in the budgets. These additional source terms will be denoted as F_{ij}^p. Moreover, in the HST-SL cases, the inhomogeneity introduced by the Stokes layers leads to the appearance of transport terms in the budget equations. However, if one focuses on the region outside the Stokes layer, the additional source terms and the transport terms become negligible (due to local homogeneity) and a direct comparison with the uncontrolled case is possible.

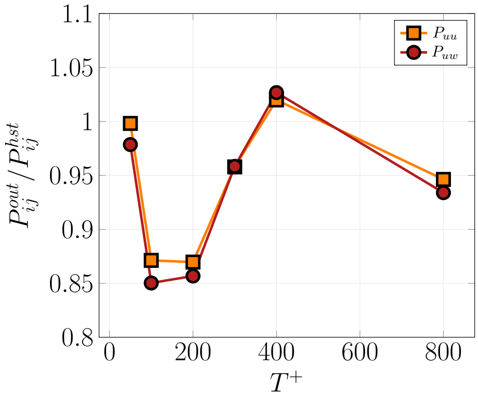

Figure 4: Production in HST-SL, measured outside SL.

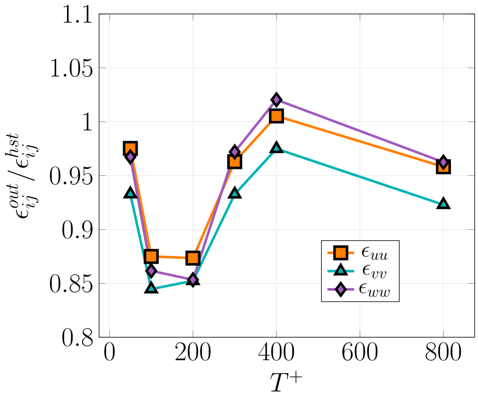

Figure 5: Dissipation in HST-SL, measured outside SL.

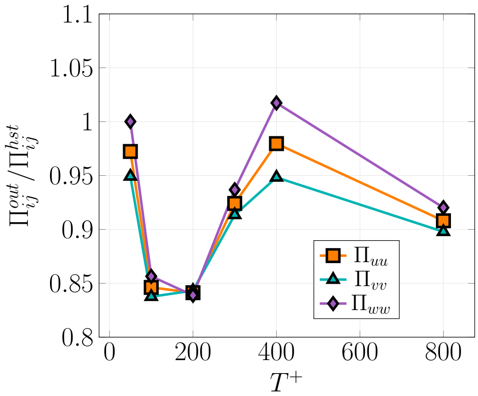

Figure 6: Pressure-strain in HST-SL, measured outside SL.

The production of turbulent kinetic energy depends on the interaction between the S and $\langle u'w' \rangle$. The link between this quantity and c_f may be readily found by considering the FIK identity (Fukagata *et al.* (2002)) or, in case of HST, Eq. 5. Physically, this is related to the interactions (sweeps and ejections, which are found also in HST, (Dong *et al.* (2017))) between streaks and quasi-streamwise-vortices. The idea is that the Stokes layer is able to inhibit such cycle, thus reducing turbulent kinetic energy production and, ultimately, friction. Fig. 4 shows the variation with the forcing period of the production terms for $\langle u'^2 \rangle$ and $\langle u'w' \rangle$. Note that these are the only non-zero terms and therefore the production of turbulent ki-

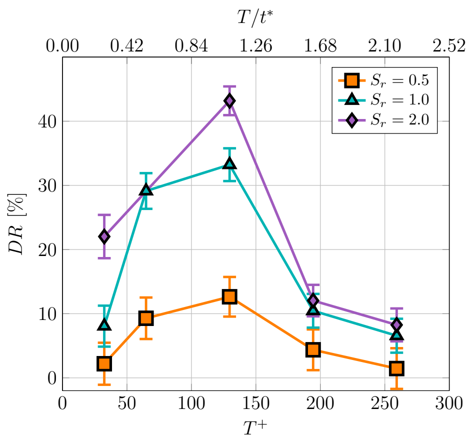

Figure 7: *DR* in HST-S2 cases.

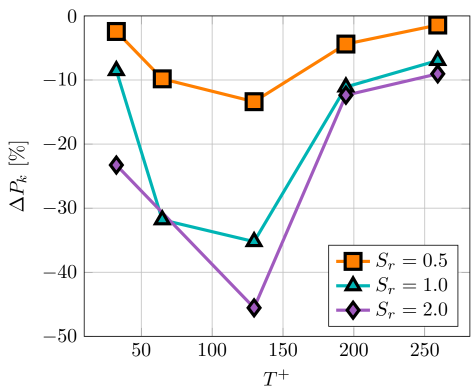

Figure 8: $\Delta P_k = P_k / P_{k,0} - 1$ in HST-S2 cases.

netic energy is given by $P_k = P_{uu}/2$. Indeed, the results show a good correlation between P_k and *DR*. Consistent with the reduction in P_k, Fig. 5 shows that the maximum *DR* coincides with a reduction in ε.

Xu & Huang (2004) and Touber & Leschziner (2012) argued that an important role in the drag reduction mechanism is played by the pressure-velocity term in the $\langle w'^2 \rangle$ budget, i.e. Π_{ww}. In fact, Π_{ww} is the only source term for $\langle w'^2 \rangle$, which in turn contributes to the production of the shear stress, i.e. $P_{uw} = -S\langle w'^2 \rangle$. Fig. 6 shows that all Π_{ij} terms correlate relatively well with *DR*. The best agreement is found with Π_{ww}, that reaches a minimum for $T^+ = 200$, while at $T^+ = 400$ becomes larger than the reference value. These results seem consistent with those of Xu & Huang (2004) and Touber & Leschziner (2012).

HST-S2 cases

Fig. 7 reports the variation of *DR* wrt. the actuation parameters for the HST-S2 cases, i.e. T^+ and S_r. As for the HST-SL cases, for a set value of S_r, *DR* varies non-monotonically with T^+. It is remarkable that both in HST-SL (Fig. 2) and HST-S2 cases (Fig. 7) the maximum drag reduction is obtained for a forcing period corresponding to the eddy turnover time t^*. Instead, for a fixed value of T^+, *DR* grows monotonically with S_r. These results are consistent with the effect of spanwise forcing in channel flows (Quadrio & Ricco (2004)).
With the HST-S2 approach the flow remains statistically homogeneous in all directions even when forcing is applied. As a consequence, unlike the HST-SL cases, no transport terms

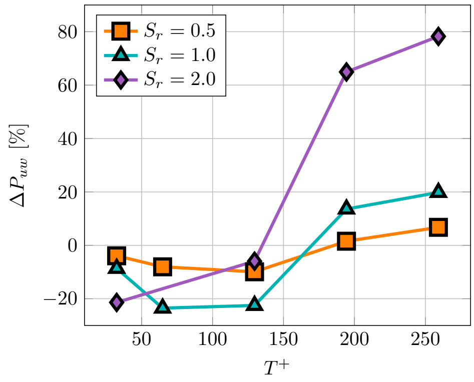

Figure 9: $\Delta P_{uw} = P_{uw} / P_{uw,0} - 1$ in HST-S2 cases.

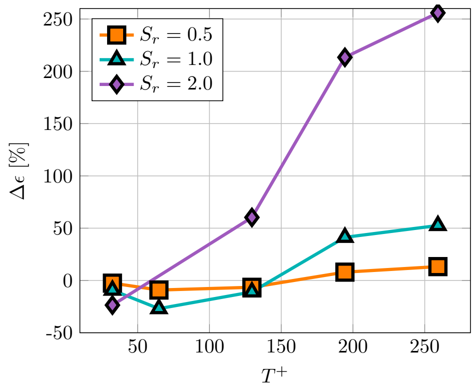

Figure 10: $\Delta\varepsilon = \varepsilon_k / \varepsilon_{k,0} - 1$ in HST-S2 cases.

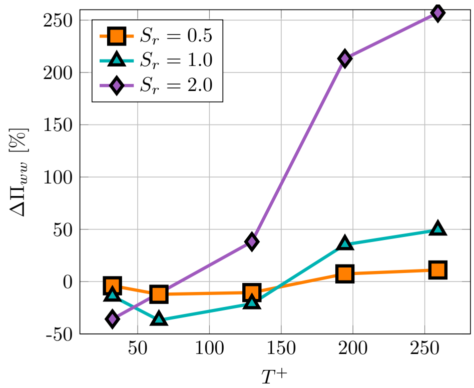

Figure 11: $\Delta\Pi_{ww} = \Pi_{ww} / \Pi_{ww,0} - 1$ in HST-S2 cases.

appear in the budgets, thus allowing for a clearer comparison with the uncontrolled case. Clearly, also in HST-S2 cases control introduces additional source terms F^p_{ij} in the budgets, as discussed before.

Fig. 8 shows the variations of P_k with the actuation parameters in the HST-S2 cases. As expected, a strong correlation with *DR* is observed, consistent with Fig. 4 and the idea of suppression of sweeps and ejections by the spanwise shear. P_{uw}, reported in Fig. 9, shows a different behavior. The period at which the maximum reduction in P_{uw} is measured decreases from $T^+ \approx 128$ at $S_r = 0.5$, to $T^+ \approx 64$ and $T^+ \approx 32$ for $S_r = 1$ and $S_r = 2$, respectively. The effect of forcing on ε is reported in Fig. 10. An important difference wrt. P_k is that ε changes non-monotonically with S_r, with the maximum reduction in ε measured at $S_r = 1$. Moreover, the highest depletion in ε is observed for $T^+ \approx 64$, for $S_r = 0.5$ and $S_r = 1$, and $T^+ \approx 32$ for $S_r = 2$, rather than the value of $T^+ \approx 128$ at which the maximum of *DR* occurs.

The imbalance between ε and P_k is equal to the additional source term F_k^p, introduced by the spanwise forcing. Note that, since ε must balance the total power input, i.e. the sum of P_k and F_k^p, a negative value of $\Delta\varepsilon$ implies a net power saving.

Fig. 11 reports the variation of Π_{ww} with the actuation parameters in the HST-S2 cases. Consistent with the HST-SL cases and the results of Xu & Huang (2004) and Touber & Leschziner (2012), large *DR* cases generally correspond to a depletion of Π_{ww}. However, it should be noted that $\Delta\Pi_{ww}$ closely resembles $\Delta\varepsilon$, rather than *DR*. Indeed, the budget equation for $\overline{w^2}$, in HST-S2 cases, simply reduces to $\Pi_{ww} = \varepsilon_{ww}$. If one uses the classical isotropic dissipation assumption, the budget reduces to $\Pi_{ww} \approx 2/3\varepsilon$, thus explaining the similarities between Fig. 10 and Fig. 11.

CONCLUSION

This study demonstrates that removing the physical wall and applying spanwise forcing in homogeneous shear turbulence (HST) could offer a viable numerical configuration to isolate the physics of drag reduction mechanisms. Both the HST-SL and the HST-S2 approaches yielded results, both in terms of *DR* and other statistical quantities commonly used in investigating spanwise forcing, consistent with conventional wall-bounded flows.

An optimal forcing period exists, which corresponds to the eddy turnover time t^*, suggesting that the interaction between spanwise shear and larger turbulent structures is central to the drag reduction mechanism. The analysis of budget terms revealed a strong correlation between *DR* and the suppression of P_k, supporting the hypothesis that spanwise forcing inhibits the sweep and ejection cycle, ultimately responsible for skin friction.

Furthermore, the HST-S2 approach proved particularly effective for analysis, as it maintained statistical homogeneity, thereby eliminating transport terms and allowing for a clearer comparison of energy budgets against the uncontrolled case. These results indicate that HST may serve as an effective simplified model for elucidating the physical mechanisms responsible for turbulent drag reduction.

REFERENCES

Agostini, L., Touber, E. & Leschziner, M.A. 2014 Spanwise oscillatory wall motion in channel flow: drag-reduction mechanisms inferred from DNS-predicted phase-wise property variations at $Re_{\tau} = 1000$. *Journal of Fluid Mechanics* **743**, 606–635.

Agostini, L., Touber, E. & Leschziner, M. A. 2015 The turbulence vorticity as a window to the physics of friction-drag reduction by oscillatory wall motion. *International Journal of Heat and Fluid Flow* **51**, 3–15.

Corrsin, S. 1958 Local isotropy in turbulent shear flow. NTRS Author Affiliations: Johns Hopkins University NTRS Report/Patent Number: NACA-RM-58B11 NTRS Document ID: 19930089981 NTRS Research Center: Legacy CDMS (CDMS).

Dong, S., Lozano-Durán, A., Sekimoto, A. & Jiménez, J. 2017 Coherent structures in statistically stationary homogeneous shear turbulence. *Journal of Fluid Mechanics* **816**, 167–208.

Duque-Daza, C. A., Baig, M. F., Lockerby, D. A., Chernyshenko, S. I. & Davies, C. 2012 Modelling turbulent skin-friction control using linearized Navier–Stokes equations. *Journal of Fluid Mechanics* **702**, 403–414.

Fukagata, K., Iwamoto, K. & Kasagi, N. 2002 Contribution of Reynolds stress distribution to the skin friction in wall-bounded flows. *Physics of Fluids* **14** (11), L73–L76, tex.catalog: 00353 tex.myfile: file:///home/mq/Library/fukagata-iwamoto-kasagi-2002.pdf.

Gualtieri, P., Casciola, C. M., Benzi, R., Amati, G. & Piva, R. 2002 Scaling laws and intermittency in homogeneous shear flow. *Physics of Fluids* **14** (2), 583–596.

Jung, W. J., Mangiavacchi, N. & Akhavan, R. 1992 Suppression of turbulence in wall-bounded flows by high-frequency spanwise oscillations. *Physics of Fluids A: Fluid Dynamics* **4** (8), 1605–1607.

Lee, M. J., Kim, J. & Moin, P. 1990 Structure of turbulence at high shear rate. *Journal of Fluid Mechanics* **216**, 561–583.

Luchini, P. 2021 Introducing CPL. *2012.12143* .

Luchini, P. & Quadrio, M. 2006 A low-cost parallel implementation of direct numerical simulation of wall turbulence. *Journal of Computational Physics* **211** (2), 551–571.

Mansour, N., Kim, J. & Moin, P. 1988 Reynolds-stress and dissipation-rate budgets in a turbulent channel flow. *Journal of Fluid Mechanics* **194**, 15–44, tex.myfile: file:///home/mq/Library/mansour-kim-moin-1988.pdf.

Pumir, A. 1996 Turbulence in homogeneous shear flows. *Physics of Fluids* **8** (11), 3112–3127.

Quadrio, M. & Ricco, P. 2004 Critical assessment of turbulent drag reduction through spanwise wall oscillation. *Journal of Fluid Mechanics* **521**, 251–271.

Quadrio, M. & Sibilla, S. 2000 Numerical simulation of turbulent flow in a pipe oscillating around its axis. *Journal of Fluid Mechanics* **424**, 217–241, tex.catalog: 0103 tex.myfile: file:///home/mq/Library/quadrio-sibilla-2000.pdf.

Ricco, P., Ottonelli, C., Hasegawa, Y. & Quadrio, M. 2012 Changes in turbulent dissipation in a channel flow with oscillating walls. *Journal of Fluid Mechanics* **700**, 77–104.

Rogallo, R.S. 1981 Numerical Experiments in Homogeneous Turbulence. TM 81315. NASA, tex.catalog: 00195.

Sekimoto, A., Dong, S. & Jiménez, J. 2016 Direct numerical simulation of statistically stationary and homogeneous shear turbulence and its relation to other shear flows. *Physics of Fluids* **28** (3), 035101.

Touber, E. & Leschziner, M.A. 2012 Near-wall streak modification by spanwise oscillatory wall motion and drag-reduction mechanisms. *Journal of Fluid Mechanics* **693**, 150–200, tex.myfile: file:///home/mq/Library/touber-leschziner-2012.pdf.

Xu, C.-X. & Huang, W.-X. 2004 Transient response of Reynolds stress transport to spanwise wall oscillation in a turbulent channel flow. *Physics of Fluids* **17** (1), 018101–018101–4.

Yakeno, A., Hasegawa, Y. & Kasagi, N. 2014 Modification of quasi-streamwise vortical structure in a drag-reduced turbulent channel flow with spanwise wall oscillation. *Physics of Fluids* **26**, 085109.